Hot-Wire Investigation of an Unseparated Shock-Wave/Turbulent Boundary-Layer Interaction

K. Hayakawa,* A. J. Smits,† and S. M. Bogdonoff‡
Princeton University, Princeton, New Jersey

Detailed hot-wire measurements of the longitudinal component of the mass-flow fluctuations have been made for an adiabatic fully attached shock-wave/turbulent boundary-layer interaction. The shock wave is induced by an 8-deg compression corner at a Mach number of 2.85 and a unit Reynolds number of 6.3×10^7 m^{-1}. The data indicate that the absolute mass-flow turbulence intensity increases abruptly through the shock wave, and continues to increase with further distance downstream. When nondimensionalized by the local freestream mass-flow rate the maximum turbulence intensity actually exceeds the upstream equilibrium value at the last measurement station. Measurements of the probability density of the fluctuations reveal only minor difference between the boundary-layer behavior upstream and downstream of the shock. A significant dip in the kurtosis was observed near the point of maximum intensity, which also coincided with the onset of intermittency.

Nomenclature

e = extra strain rate
M = Mach number
p = static pressure
U,u' = velocity in x direction, mean and fluctuating
x = distance along model surface measured from corner, taken as positive in the downstream direction
y = distance normal to model surface
γ = specific heat ratio or intermittency factor
δ = 99% boundary-layer thickness
π = wake parameter
ρ = density
$\overline{\rho U}$ = mean mass-flow rate
$(\rho u)'$ = fluctuating mass-flow rate
$\langle\ \rangle$ = root mean square value

Subscripts

E = local freestream condition
ref = freestream condition upstream of shock wave
0 = incoming or undisturbed condition
1 = condition upstream of shock wave
2 = condition downstream of shock wave

Introduction

In recent years increasing emphasis has been placed on developing numerical techniques to predict turbulent boundary-layer behavior. Although tremendous advances have been made, the prediction of complex flows, such as shock-wave/boundary-layer interactions, is still far from satisfactory. This is largely due to inadequate modeling of the turbulence behavior. These turbulence models can only be improved by investigating the physical details of turbulence over a wide range of conditions. Unfortunately, with only some exceptions,[1-9] the available experimental studies have been restricted to measurements of the mean flow properties.

The present investigation represents the first part of a parametric study of the turbulence behavior in compression-corner interactions, ranging from fully attached to separated. A constant-temperature hot-wire anemometer was used to obtain the longitudinal component of the mass-flow fluctuations. The raw data are available from the authors.[10] Of course, mass-flow fluctuation data by themselves may not provide sufficient information to improve existing turbulence models. The present results, however, should be useful in understanding the basic physics of shock-wave/turbulent boundary-layer interactions and should also serve as a data base for checking the validity of various calculation methods. (Further hot-wire measurements, including measurements of Reynolds stresses, are currently under way to aid more directly in formulating turbulence models.) The present results include the first available measurements of probability density and higher moments of mass-flow fluctuations through a shock-wave/boundary-layer interaction. Some aspects of the intermittency behavior are also discussed.

Experimental Technique

Wind Tunnel Test Conditions

The investigation was carried out in the Princeton University 20×20 cm high Reynolds number supersonic wind tunnel. The 8-deg compression corner was installed on the tunnel floor, and aerodynamic fences were attached to both sides of the model to ensure two dimensionality of the flow (see Fig. 1). The freestream Mach number was 2.85, the unit Reynolds number was approximately 6.3×10^7/m, and the wall conditions were near adiabatic. The rms freestream turbulence level, expressed as a fraction of the freestream mass-flow rate, was about 1%. The incoming two-dimensional turbulent boundary layer developed in a zero pressure gradient and the overall thickness δ_0 was about 26 mm. Mean flow measurements and surface oil flow visualization indicated that the flow remained fully attached throughout the interaction.[11]

Hot-Wire Measurement Technique

A DISA 55M10 constant-temperature anemometer was used to measure the streamwise component of the mass-flow fluctuations. Probes were constructed by welding 5-μm tungsten wires to stainless steel support prongs. Some slack was given to the wire to avoid strain-gaging, and the wire

Presented as Paper 82-0985 at the AIAA/ASME Third Joint Thermophysics, Fluids, Plasma, and Heat Transfer Conference, St. Louis, Mo., June 7-11, 1982; submitted June 11, 1982; revision received June 16, 1983.

*Research Associate, Gas Dynamics Laboratory, Mechanical and Aerospace Engineering Department. Member AIAA.
†Assistant Professor, Mechanical and Aerospace Engineering Department. Member AIAA.
‡Professor, Mechanical and Aerospace Engineering Department. Fellow AIAA.

length was typically 1 mm. The wires were calibrated for mass-flow sensitivity in a small Mach 3 pilot tunnel by changing the tunnel stagnation pressure. The temperature dependence of the mass-flow sensitivity was determined by repeating the calibration at several different resistance ratios. The operating overheat ratio varied between 1.0 and 1.3. Preliminary tests had shown that at these overheat ratios the contribution of the temperature fluctuations to the total signal was small and, subsequently, it was neglected. The system frequency response (deduced from a square-wave test) was typically 150 kHz or better.

The wires were not calibrated in the subsonic and transonic regimes, and the calibration is valid only when the local Mach number exceeds 1.2, where the mass-flow sensitivity is independent of Mach number.[12] The sonic line in the present flow, however, lies very close to the wall throughout the interaction.

Following appropriate filtering, the mean and fluctuating components of the hot-wire signal were digitized directly at sampling rates of 50 and 500 kHz, respectively, and the raw data were stored on-line in the memory of a Hewlett-Packard HP1000 minicomputer for further processing. At each measurement point, data were taken as an ensemble of 25 records, each of which contained 1024 sampled points. Satisfactory convergence of fluctuation data was achieved with this record length (within 1% at $y/\delta=0.5$). The instantaneous values of the anemometer voltage were directly converted to the instantaneous values of mass flow by inverting the calibration curve, thereby avoiding the use of sensitivity coefficients. The instantaneous mass-flow fluctuations were found by subtracting the time-averaged mass flow from the total instantaneous mass flow.

Hot-wire traverses were made at 5 stations upstream of the corner and 18 stations downstream of the corner. The measurement stations were closely spaced in the vicinity of the corner to give a detailed survey of the interaction region.

Repeatability of the measurements was checked at a number of stations and was found to be excellent when the measurement was repeated using the same wire. Disagreement of up to $\pm 5\%$, however, was found when different wires were used. The reasons for these discrepancies are currently under investigation.

After each traverse, the wires were checked for strain gaging, and those found to be suspect were discarded. A series of tests was carried out to evaluate the effect of probe interference on the flow. Flow visualization results showed that all the waves generated by the probe were swept downstream and no probe effect was detected in the wall static pressure upstream of the measurement station.

The difficulties of making hot-wire measurements in high-speed flows are well known. Nevertheless, an error analysis[10] indicated that the error in $\langle(\rho u)'\rangle$ upstream of the shock wave was less than approximately $\pm 10\%$. Downstream of the shock wave this error increases somewhat, but it is unlikely to exceed $\pm 15\%$.

Results and Discussion

Mean Flowfield

The detailed mean-flow measurements are reported in Refs. 11 and 13. Figure 2 shows the surface static pressure distribution and the local skin-friction coefficient behavior. The pressure begins to rise sharply ahead of the corner, but with very little upstream influence. This sharp rise is followed by a gradual increase in pressure and the pressure gradient becomes zero at approximately $2.5\delta_0$ downstream of the corner. The skin-friction coefficient falls rapidly at the corner, mainly as a result of the large adverse pressure gradient, but it recovers within $2\delta_0$ downstream. Further downstream it slowly increases, eventually exceeding the upstream value. The wake parameter has almost returned to its equilibrium value of 0.55 at the end of the test section ($x=6\delta_0$).

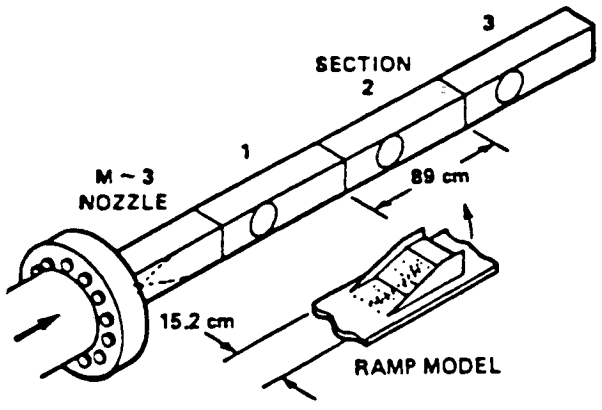

Fig. 1 Sketch of the 20×20-cm high Reynolds number channel and 8-deg ramp model.

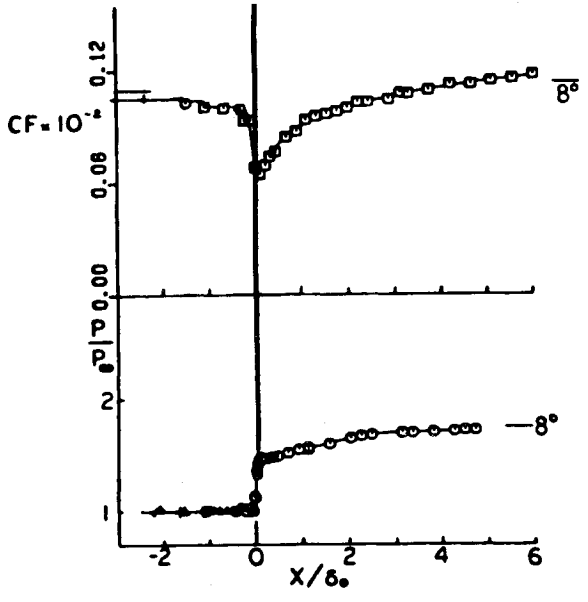

Fig. 2 Surface pressure and skin-friction coefficient distribution.

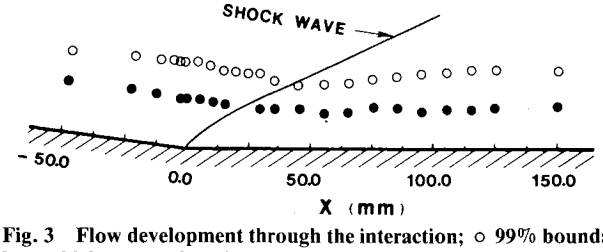

Fig. 3 Flow development through the interaction; ○ 99% boundary-layer thickness; ● location of maximum $\langle(\rho u)'\rangle$. The shock wave is indicated by the solid line.

The mean mass-flow profiles obtained by the hot wire were in good agreement with those found using a pitot tube. The 99% boundary-layer thickness determined from the hot-wire results and the location of the shock wave measured from a schlieren photograph are shown in Fig. 3. As can be seen, the boundary layer develops very slowly until it meets the shock wave. Downstream of the shock wave the boundary layer is thinner but grows more rapidly than the upstream boundary layer.

Mass-Flow Fluctuations

The rms mass-flow fluctuation level, $\langle(\rho u)'\rangle$, normalized by the freestream mass flow upstream of the shock wave, $(\rho U)_{\text{ref}}$, is shown in Fig. 4. The arrows indicate the location of

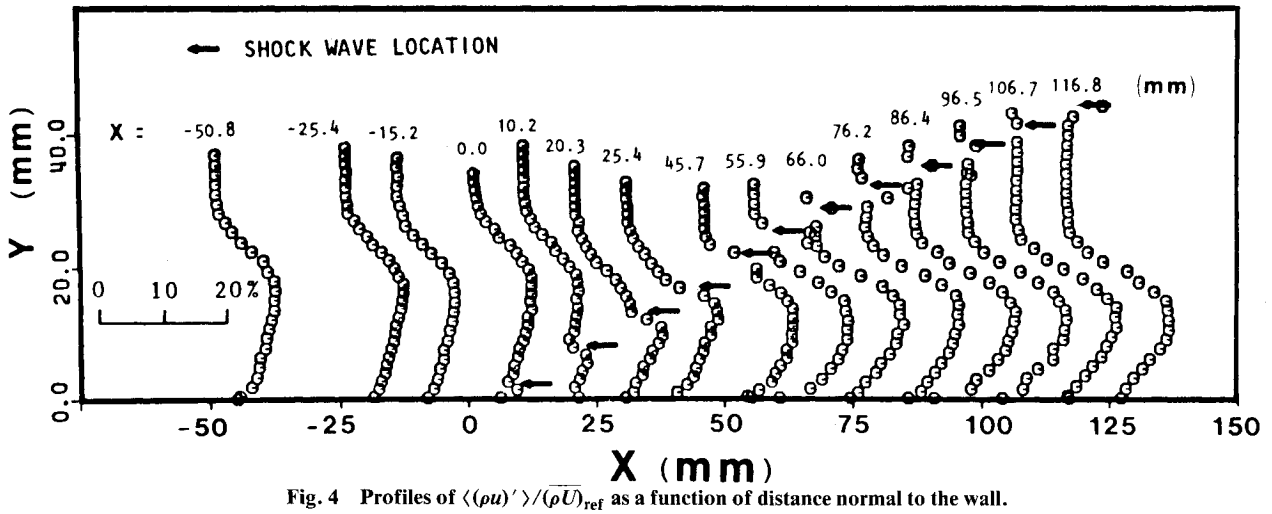

Fig. 4 Profiles of $\langle(\rho u)'\rangle/(\overline{\rho U})_{\text{ref}}$ as a function of distance normal to the wall.

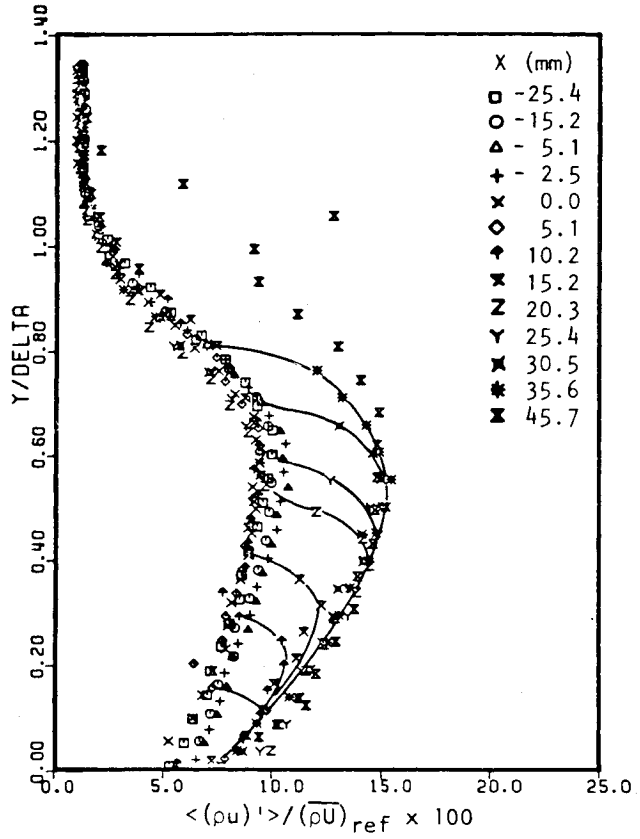

Fig. 5 Profiles of $\langle(\rho u)'\rangle/(\overline{\rho U})_{\text{ref}}$ vs y/δ, for the region close to the corner.

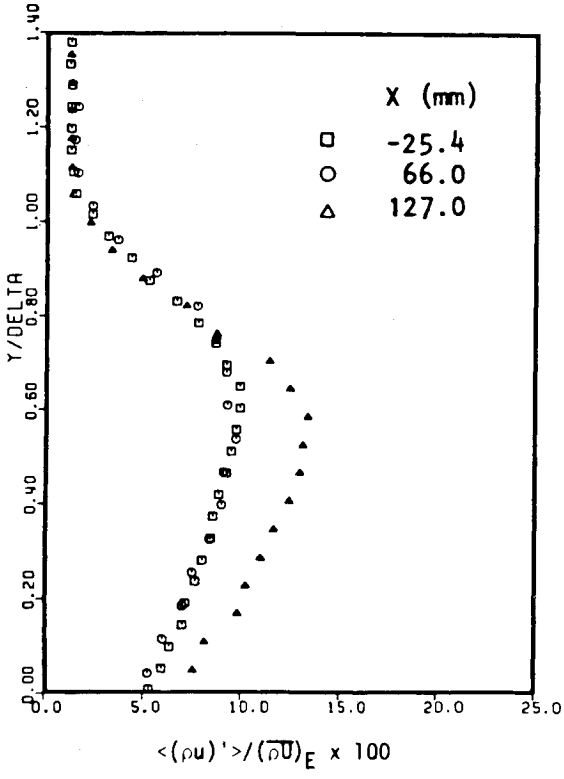

Fig. 6 Selected profiles of $\langle(\rho u)'\rangle/(\overline{\rho U})_E$, where $(\overline{\rho U})_E$ is the local freestream mass-flow rate.

the shock wave, which remains sharp and distinct almost to the wall. Further detail within the corner region is given in Fig. 5. These figures clearly show that the absolute turbulence intensity increases as soon as the flow passes through the shock wave, and that very little upstream influence is apparent. This amplification of the turbulence intensity is so dramatic that by the time the shock wave emerges from the boundary layer ($x \approx 51$ mm) the mass-flow fluctuation level, when nondimensionalized by the local freestream mass-flow rate $(\overline{\rho U})_E$, already equals its upstream equilibrium value, even though $(\overline{\rho U})_E$ increases by a factor of 1.4 through the shock. This is shown in Fig. 6, where it may also be seen that the maximum intensity continues to increase downstream. To illustrate this point further, the maximum mass-flow fluctuation level is given in Fig. 7 as a function of downstream distance, and at the end of the test section the level is seen to be still increasing.

The increase in the absolute turbulence intensity is due to viscous stresses within the shock wave, the impulse in adverse pressure gradient, as well as the short, intense exposure to extra strain rates associated with longitudinal curvature ($e = \partial v/\partial x$) and compression ($e = -\text{div } V$).[14-16]

These extra strain rates are a significant fraction of the simple shear $\partial U/\partial y$ in the present flow. For an impulsively applied strain rate the effective ratio of the extra strain rate to the mean shear may be described by the integral of the strain rate following motion of the fluid.[16] For longitudinal curvature this is equal to the total turning angle, and for compression it is given by $(1/\gamma)\ell n\ (p_2/p_1)$, where p_2/p_1 is the static pressure ratio across the shock.[17] These ratios are, respectively, 0.14 and 0.4 in the current experiment, and extra strain rates, therefore, are likely to have a significant effect on the turbulence behavior.

Smits et al.[16] showed that the effect of an impulsively applied perturbation on the dissipation length scale (or other

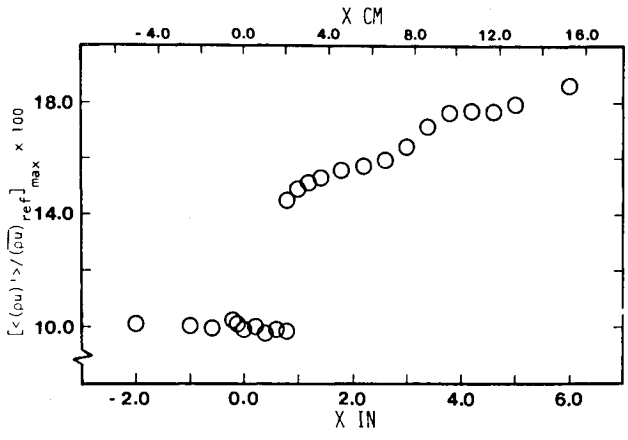

Fig. 7 Maximum value of rms mass-flow fluctuations vs distance along the wall.

structure parameter) may be simply modeled by a first-order filter function, with a gain $[1+\alpha_0 e/(\partial u/\partial y)]$, and a time constant of the order of $10\delta/U$, where 10δ is taken as a typical relaxation distance for the energy-containing eddies. The amplification factor α_0 depends on the nature of the perturbation, but is generally of order 10, and this demonstrates the importance of extra strain rates in understanding the boundary-layer behavior. Of course, the model just described relates to structural parameters rather than dimensional, derived quantities like turbulence intensity, yet the expected amplification due to presence of destabilizing extra strain rates is certainly observed.

The influence of the viscous stresses within the shock wave will be confined to the thickness of the shock, and the adverse pressure gradient and concave curvature effects are large only in the neighborhood of the shock. The perturbation closely approximates a true impulse, and it would seem possible to predict the turbulence behavior immediately downstream of the shock using rapid distortion theory. This possibility is under investigation.

A final observation may be made. There is a weak but persistent trend for the position of maximum turbulence intensity to move toward the wall as we proceed downstream (Fig. 3). The increase in turbulence production associated with the large velocity gradients near the wall (observed by Settles et al.[11]) may be responsible for this, but without further measurements this cannot be verified.

Statistical Properties of the Mass-Flow Fluctuations

In addition to the time-averaged properties of the turbulence intensities, the statistical properties of the fluctuations are also interesting. For example, the skewness of the velocity probability distributions gives some guide to the nature of the turbulence transport process, and the flatness of the distributions gives an approximate measure of intermittency.

Figure 8 shows time traces of the anemometer fluctuating voltage at various locations in the undisturbed boundary layer at $x=-25.4$ mm and the corresponding normalized probability density distributions are given in Fig. 9. The solid curve in Fig. 9 is the normalized Gaussian distribution. Each probability density distribution and higher order moment was calculated using the fluctuating values of the mass-flow rate rather than the fluctuating anemometer voltage; using the anemometer voltage introduces some error due to the nonlinear relationship between the anemometer voltage and the mass-flow rate. Use of the anemometer voltage to determine the higher order moments should therefore be avoided whenever possible. One of the advantages of digital processing is that the data processing can be performed using the mass-flow rate directly. All of the data sampled at each

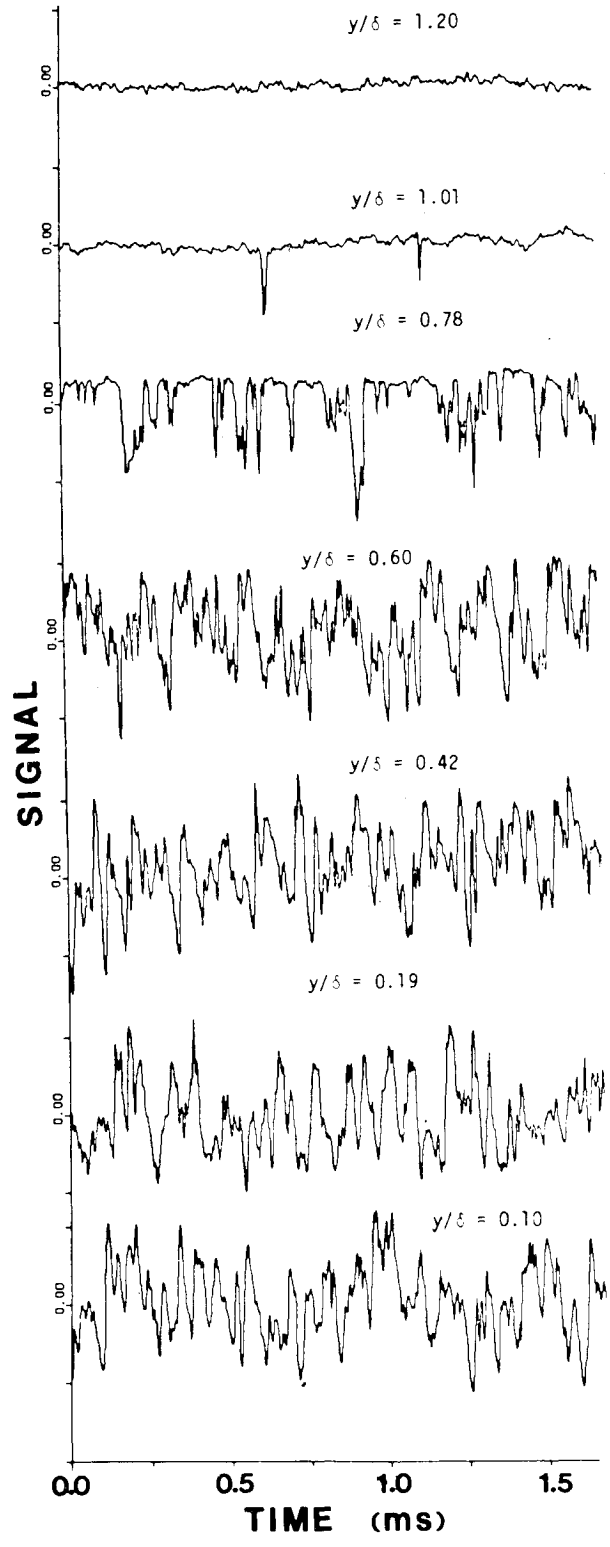

Fig. 8 Time trace of fluctuating anemometer output voltage at $x=-25.4$ mm for different locations within the boundary layer.

measurement point, i.e., 50 ms of data, were used to calculate the probability density and higher order moments. Adequate convergence was achieved with this record length.

The intermittent nature of the fluctuations is clearly seen in the outer part of the boundary layer. At $y/\delta=1.2$ the fluctuations arise entirely from the freestream and the distribution is Gaussian. At $y/\delta=1.0$ negative one-sided "spikes" start to appear sporadically on the signal trace. (For the constant temperature anemometer, the mass-flow deficit from the mean appears as negative signals on the traces.) As

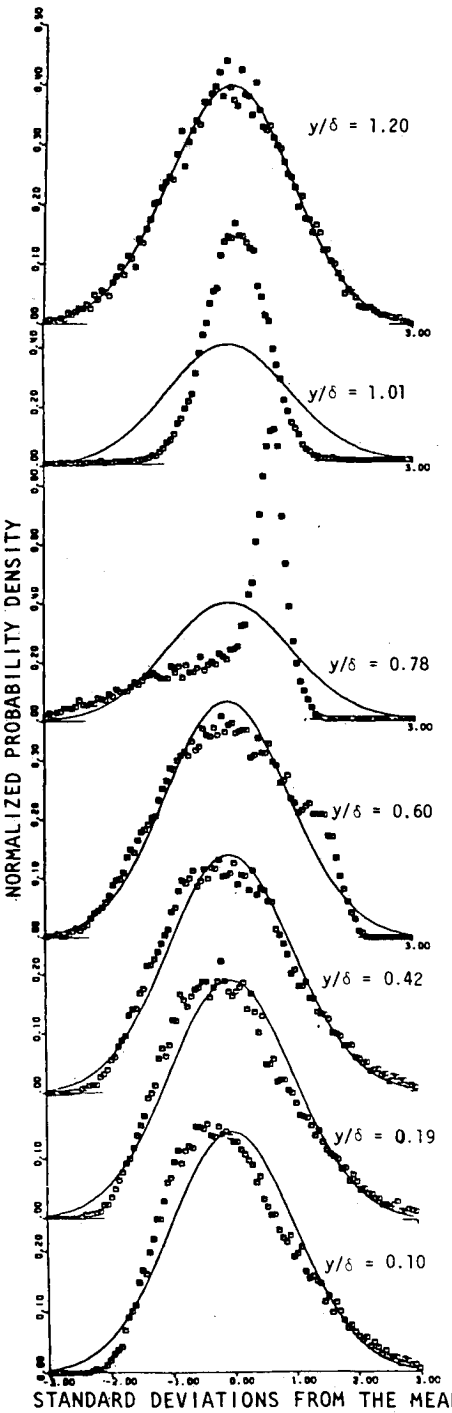

Fig. 9 Probability density distributions at $x = -25.4$ mm for different locations within the boundary layer.

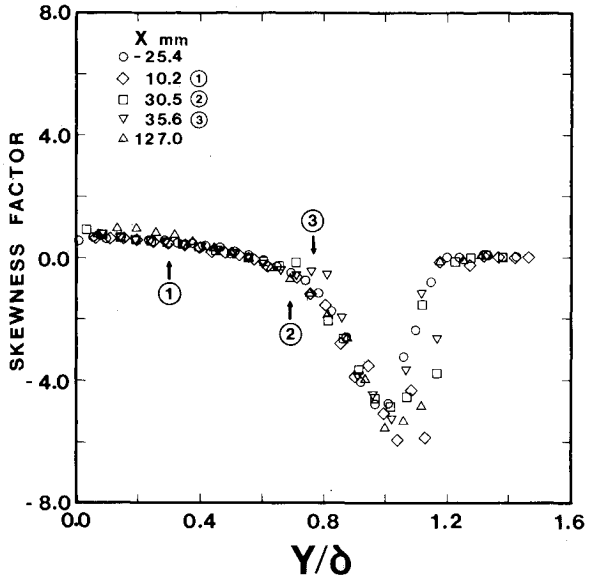

Fig. 10 Skewness factor distributions, the arrows indicate the shock-wave location.

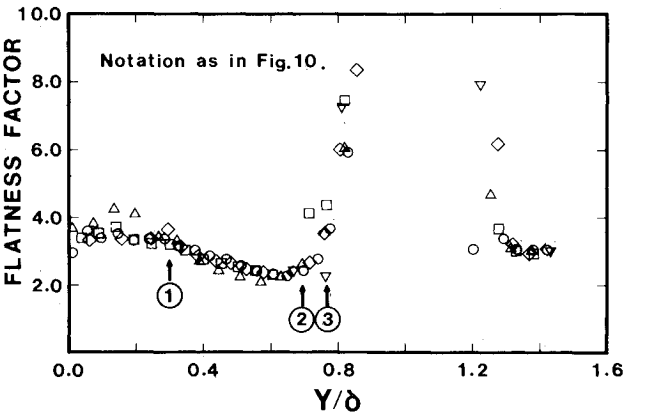

Fig. 11 Flatness factor distributions, symbols and notation as in Fig. 10.

the probe moves toward the wall, progressively more spikes appear, and at $y/\delta = 0.6$ the signal becomes almost symmetrical around the mean value. The one-sided spikes in the signal result in skewed probability density distributions; in the region $y/\delta < 0.6$ the probability density distributions are positively skewed, and the skewness increases monotonically as the wall is approached.

The dimensionless third- and fourth-order moments (skewness and flatness) of the mass-flow fluctuations at different stations are shown in Figs. 10 and 11. The shock-wave location is indicated by arrows. One remarkable result is that the dimensionless higher order moments appear to change very little through the shock wave, in spite of the sudden increase in the absolute magnitude of the mass-flow fluctuations. Downstream of the shock wave the minimum in flatness factor appears to move slightly nearer the wall. A comparison of Figs. 11 and 4 indicates that the location of the minimum flatness factor coincides with the location of maximum $\langle (\rho u)' \rangle / (\overline{\rho U})_{\text{ref}}$.

The results of Owen et al.[18] show that their skewness and flatness are zero and three, respectively, for $0.1 < y/\delta < 0.8$. The absence of such a constant Gaussian region in Figs. 10 and 11 is partly due to the use of mass-flow rate to calculate the higher moments. The higher moments of Owen et al. were evaluated by using the fluctuating component of the anemometer voltage. The use of voltage values does bring the present data closer to the "normal" values of zero and three for the skewness and flatness factor, respectively, but this ignores the nonlinearity of the voltage signal.

Yanta and Lee[19] measured u' statistics in a turbulent boundary layer similar to the present incoming flow, and found a dip in both the skewness and the flatness factor near $y/\delta = 0.7$. No such dip is observed here in the skewness distribution, but the dip in the flatness factor is much larger than that found by Yanta and Lee. It is difficult to ascribe this observation to experimental error, since both the skewness and flatness attain their expected values in the freestream. Similar flatness distributions have been measured in subsonic flows,[20,21] and these dips seem to be a general characteristic of turbulent boundary-layer behavior.

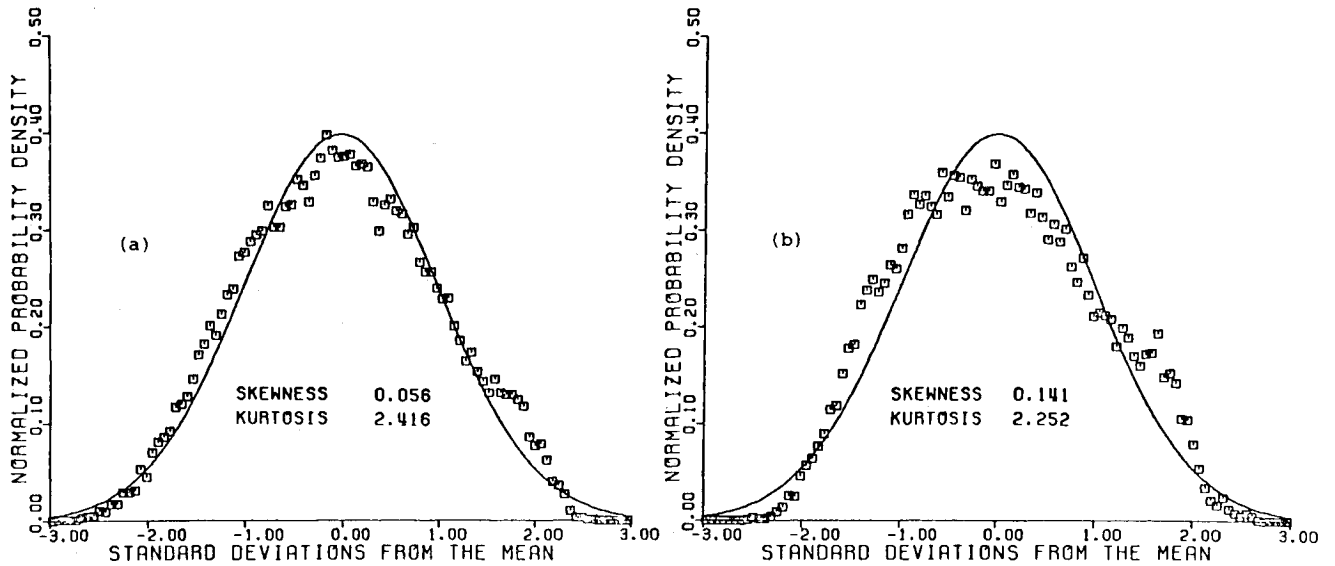

Fig. 12 Two selected probability density distributions. a) $x = -25.4$ mm, $y/\delta = 0.56$; b) $x = 127.0$ mm, $y/\delta = 0.5$.

When the flatness factor was used to determine the intermittency factor γ ($=3/$flatness factor), unrealistic values, greater than 1, result in the central portion of the boundary layer. By comparing Figs. 9 and 11 it appears that the onset of intermittency coincides approximately with the minimum found in the flatness distribution. The probability densities (Fig. 9) show that at $x = -25.4$ mm and $y/\delta = 0.6$, the mass-flow fluctuation signal contains some contribution from the freestream. The point in the boundary layer at which the intermittency becomes apparent moves slightly toward the wall as we proceed downstream of the shock wave (see Fig. 12), as does the point of minimum flatness factor and maximum turbulence intensity (Figs. 3 and 11). In Fig. 12, note that the contribution from the freestream, indicated by the bump on the right-hand side, is similar in these two profiles, although the location within the boundary layer is different. However, the overall intermittency behavior of this flow, despite some minor differences, appears to be in reasonable agreement with Klebanoff's[22] incompressible boundary-layer data, but in sharp disagreement with Owen et al.,[18] who found that in a hypersonic boundary layer the intermittent nature of the outer flow only became important for $y/\delta > 0.8$. Thus, in the present flow, Mach number effects in the intermittency behavior do not appear to be significant.

Summary of Conclusions

The absolute mass-flow turbulence intensity under the action of the sudden compression and a concave curvature impulse increases rapidly downstream of the shock wave. The intensity level, scaled by the local freestream mass-flow rate, actually equals the upstream equilibrium values by the time the shock wave has emerged from the boundary layer and continues to increase downstream.

It was suggested that the present flow is a good candidate for a rapid distortion calculation, in that the shock wave closely represents a true impulse.

On examining the statistics of the mass-flow fluctuations it was found that both the skewness and flatness distributions are relatively unaffected by the interaction of the shock wave with the boundary layer. The onset of intermittency in the outer flow, despite some minor differences, did not show significant Mach number effects when compared with incompressible boundary-layer data.

Acknowledgments

This work was supported partly by the U.S. Air Force Office of Scientific Research under Contract F49620-81-K-0018, monitored by Dr. J. D. Wilson and partly by NASA under Grant NAGW-240 monitored by Dr. G. Hicks. Our thanks go to Drs. D. R. Williams, G. S. Settles, and K. C. Muck for many useful discussions.

References

[1]Rose, W. C., "The Behavior of a Compressible Turbulent Boundary Layer in a Shock-Wave Induced Adverse Pressure Gradient," NASA TN D-7092, March 1973.

[2]Rose, W. C. and Johnson, D. A., "A Study of Shock-Wave Turbulent Boundary Layer Interaction Using Laser Velocimeter and Hot-Wire Anemometer Techniques," AIAA Paper 74-95, 1974.

[3]Rose, W. C., "Turbulent Measurements in a Compressible Boundary Layer," *AIAA Journal*, Vol. 12, Aug. 1974, pp. 1060-1064.

[4]Mikulla, V. and Horstman, C. C., "Turbulent Measurements in Hypersonic Shock-Wave Boundary-Layer Interaction Flows," AIAA Paper 76-162, 1976.

[5]Mateer, G. G., Brosh, A., and Viegas, J. R., "A Normal Shock-Wave Turbulent Boundary-Layer Interaction at Transonic Speeds," AIAA Paper 76-161, 1976.

[6]Ardonceau, P., Lee, D. H., Alziary de Roquefort, T., and Goethals, R., "Turbulence Behavior in Shock Wave/Boundary Layer Interaction," *Turbulent Boundary Layers—Experiments, Theory and Modelling*, NATO AGARD CP-271, 1979, pp. 8.1-14.

[7]Lee, D. H., "Etude de l'evolution de la turbulence dans une interaction onde de choc-couche limite," Doctorate Thesis, The University of Poitiers, June 1979.

[8]Kussoy, M. I., Viegas, J. R., and Horstman, C. C., "Investigation of a Three-Dimensional Shock Wave Separated Turbulent Boundary Layer," *AIAA Journal*, Vol. 18, Dec. 1980, pp. 1477-1484.

[9]Settles, G. S., Baca, B. K., Williams, D. R., and Bogdonoff, S. M., "A Study of Reattachment of a Free Shear Layer in Compressible Turbulent Flow," AIAA Paper 80-1408, 1980.

[10]Hayakawa, K. and Smits, A. J., "Compilation of Turbulence Data for an 8° Compression Corner at Mach 2.9—Normal Wire Data," Princeton University MAE Rept. 1600, March 1983.

[11]Settles, G. S., Fitzpatrick, T. J., and Bogdonoff, S. M., "Detailed Study of Attached and Separated Compression Corner Flowfields in High Reynolds Number Supersonic Flow," *AIAA Journal*, Vol. 17, June 1979, pp. 579-585.

[12]Kovasznay, L. S. G., "The Hot-Wire Anemometer in Supersonic Flow," *Journal of the Aeronautical Sciences*, Vol. 17, Sept. 1950, pp. 565-573.

[13]Settles, G. S., Gilbert, R. B., and Bogdonoff, S. M., "Data Compilation for Shock Wave/Turbulent Boundary Layer Interaction Experiments on Two-Dimensional Compression Corners," Princeton University MAE Rept. 1489, Aug. 1980.

[14]Bradshaw, P., "Effects of Streamline Curvature on Turbulent Flow," AGARDograph 169, 1973.

[15]Bradshaw, P., "The Effect of Mean Compression or Dilatation on the Turbulence Structure of Supersonic Boundary Layers," *Journal of Fluid Mechanics,* Vol. 63, 1974, pp. 449-464.

[16]Smits, A. J., Young, S. T. B., and Bradshaw, P., "The Effect of Short Regions of High Surface Curvature on Turbulent Boundary Layers," *Journal of Fluid Mechanics,* Vol. 94, 1979, pp. 209-242.

[17]Hayakawa, K., Smits, A. J., and Bogdonoff, S. M., "Turbulence Measurements in Two Shock-Wave/Shear-Layer Interactions," *Proceedings of the Symposium on Structure of Complex Turbulent Shear Flow,* I.U.T.A.M., Springer-Verlag, 1983, pp. 279-288.

[18]Owen, F. K., Horstman, C. C., and Kussoy, M. I., "Mean and Fluctuating Flow Measurements of a Fully-Developed, Non-adiabatic, Hypersonic Boundary Layer," *Journal of Fluid Mechanics,* Vol. 70, 1975, pp. 393-413.

[19]Yanta, W. J. and Lee, R. E., "Measurements of Mach 3 Turbulence Transport Properties on a Nozzle Wall," *AIAA Journal,* Vol. 14, June 1976, pp. 725-729.

[20]Hancock, P. E., "The Effect of Freestream Turbulence on Turbulent Boundary Layers," Ph.D. Thesis, Imperial College, University of London, 1980.

[21]Muck, K. C., "Turbulent Boundary Layers on Mildly Curved Surfaces," Ph.D. Thesis, Imperial College, University of London, Jan. 1982.

[22]Klebanoff, P. S., "Characteristics of Turbulence in a Boundary Layer with Zero Pressure Gradient," NACA TR-1247, 1955.